Small-sized gadolinium oxide based nanoparticles for high-efficiency theranostics of orthotopic glioblastoma

Zheyu Shen[a,b], **Ting Liu**[e], **Zhen Yang**[b], **Zijian Zhou**[b], **Wei Tang**[b], **Wenpei Fan**[d], **Yijing Liu**[b], **Jing Mu**[b], **Ling Li**[b], **Vladimir I. Bregadze**[f], **Swadhin K. Mandal**[g], **Anna A. Druzina**[f], **Zhenni Wei**[a], **Xiaozhong Qiu**[c], **Aiguo Wu**[a], **Xiaoyuan Chen**[b]

[a]Cixi Institute of Biomedical Engineering, CAS Key Laboratory of Magnetic Materials and Devices, Key Laboratory of Additive Manufacturing Materials of Zhejiang Province, Ningbo Institute of Materials Technology and Engineering, Chinese Academy of Sciences, 1219 Zhong-guan West Road, Ning-bo, Zhe-jiang 315201, China.

[b]Laboratory of Molecular Imaging and Nanomedicine, National Institute of Biomedical Imaging and Bioengineering, National Institutes of Health, Bethesda, Maryland 20892, USA.

[c]Guangdong Provincial Key Laboratory of Construction and Detection in Tissue Engineering, Biomaterials Research Center, School of Biomedical Engineering, Southern Medical University, Guangzhou, 510515, China

[d]State Key Laboratory of Natural Medicines and Jiangsu Key Laboratory of Drug Discovery for Metabolic Diseases, Center of Advanced Pharmaceuticals and Biomaterials, China Pharmaceutical University, Nanjing, 210009, PR China

[e]State Key Laboratory of Molecular Vaccinology and Molecular Diagnostics & Center for Molecular Imaging and Translational Medicine, School of Public Health, Xiamen University, Xiamen, 361102, China.

[f]A.N. Nesmeyanov Institute of Organoelement Compounds of Russian Academy of Sciences, Vavilov Str. 28, Moscow 119991, Russia.

[g]Department of Chemical Sciences, Indian Institute of Science Education and Research-Kolkata, Mohanpur-741246, India.

Abstract

Glioblastoma (GBM) is one of the most malignant tumors with poor prognosis and outcomes. Although smaller particle size can lead to higher blood-brain barrier (BBB)-permeability of the nanomaterials, most of the reported BBB-crossable nanomaterials for targeted GBM therapy are

Corresponding Authors: shawn.chen@nih.gov (X. Chen), aiguo@nimte.ac.cn (A. Wu), qqiuxzh@163.com (X. Qiu), wenpei.fan@cpu.edu.cn (W. Fan).

The authors declare no competing financial interest.

Appendix A. Supplementary data

Supplementary data related to this article can be found at http://www.journals.elsevier.com/biomaterials.

larger than 24 nm. To realize theranostics of GBM, co-loading of therapeutic and diagnostic agents on the same nanomaterials further results in larger particle size. In this study, we developed a kind of novel BBB-transportable nanomaterials smaller than 14 nm for high-efficiency theranostics of GBM (*i.e.*, high contrast magnetic resonance imaging (MRI) and radiosensitization of GBM). Typically, poly(acrylic acid) (PAA) stabilized extremely small gadolinium oxide nanoparticles with modification of reductive bovine serum albumin (ES-GON-rBSA) was synthezed in water phase, resulting in excellent water-dispersibility. RGD dimer (RGD2, Glu-{Cyclo[Arg-Gly-Asp-(D-Phe)-Lys]}$_2$) and lactoferrin (LF) were then conjugated to the ES-GON-rBSA to obtain composite nanoparticle ES-GON-rBSA-LF-RGD2 with extraordinary relaxivities (r_1 = 60.8 mM^{-1} s^{-1}, r_2/r_1 = 1.1). The maximum signal enhancement (SNR) for T_1-weighted MRI of tumors reached up to 423 ± 42 % at 12 h post-injection of ES-GON-rBSA-LF-RGD2, which is much higher than commercial Gd-chelates (< 80%). ES-GON-rBSA-LF-RGD2 exhibited high biocompatibility and can transport across the *in vitro* BBB model and the *in vivo* BBB of mice due to its small particle size (d_h = 13.4 nm) and LF receptor mediated transcytosis. Orthotopic GBM studies reinforce that ES-GON-rBSA3-LF-RGD2 can accumulate in the orthotopic GBM and enhance the radiation therapy of GBM as an effective radiosensitizing agent.

Keywords

small-sized gadolinium oxide based nanoparticles; blood-brain barrier; high contrast magnetic resonance imaging; radiosensitization; orthotopic glioblastoma

1. Introduction

Glioblastoma (GBM) is a primary malignant tumor that locates in intracranial central nervous system (CNS).[1] GBM is the highest grade glioma (grade IV) that can easily invade surrounding normal tissues resulting poor prognosis.[2] Even after careful treatments including surgical resection, chemotherapy and/or radiation therapy, the median survival of GBM-bearing patients is only around 15 months, and the five year survival rate is lower than 5 %.[2–4]

Temozolomide (TMZ) is the first line anti-GBM drug, but over 45 % of GBM may be resistant to TMZ.[5,6] Althouth there are many other anti-GBM drugs that have been tested in clinical trials, most of them failed to improve the poor prognosis due to the existance of blood-brain barrier (BBB).[7] The anti-GBM drugs are difficult to enter the brain because the BBB controls the transportation of ions and nutrients from blood circulation to brain, but prevents most therapeutic drugs from passing into the brain.[3,7]

In order to enhance the delivery of anti-GBM drugs to intracranial CNS, various BBB-crossing strategies have been developed based on nanomaterials,[8] including receptor mediated BBB-crossing,[9,10] shuttle peptide mediated BBB-crossing,[11] cell penetrating peptide (CPP) mediated BBB-crossing,[12] and cells mediated BBB-crossing.[13] For example, B. Shi *et al.* developed a kind of ROS-responsive siRNA nanomaterials (3I-NM@siRNA) functionalized with angiopep-2 peptide (37.8 nm) for targeted GBM therapy, which was prepared by complexation between poly(ethylene glycol)-block-poly[(N-(3-methacrylamidopropyl) guanidinium-co-4-(4,4,5,5-tetramethyl-1,3,2-dioxaborolan-2-

yl)benzyl acrylate)] (PEG-b-P(Gu/Hb))/Ang-poly(ethylene glycol)-block-poly(N-(3-methacrylamidopropyl) guanidinium) (Ang-PEG-b-PGu) and siRNA.[14] B.A. Tannous *et al.* developed a cyclic peptide iRGD-conjugated solid lipid nanoparticle (SLN) to deliver small interfering RNAs (siRNAs) (24.1 nm) against both epidermal growth factor receptor (EGFR) and PD-L1 for combined targeted and immunotherapy against GBM.[4] Z. Zhong *et al.* reported apolipoprotein E peptide-conjugated chimeric polymersomes (> 40 nm) that can mediate a high-efficiency GBM therapy.[15]

Although smaller particle size can lead to higher BBB-permeability of the nanomaterials based on the above-mentioned BBB-crossing strategies,[3,16] most of the reported BBB-crossable nanomaterials for targeted GBM therapy are larger than 24 nm.[4,14,15] To realize theranostics of GBM, co-loading of therapeutic and diagnostic agents on the same nanomaterials further results in larger particle size.

In this study, we developed a kind of novel BBB-transportable nanomaterials smaller than 14 nm for high-efficiency theranostics of GBM (*i.e.*, high contrast magnetic resonance imaging (MRI) and radiosensitization of GBM). Typically, poly(acrylic acid) (PAA) stabilized extremely small gadolinium oxide nanoparticles with modification of reductive bovine serum albumin (ES-GON-rBSA) was first synthezed in water phase, resulting in excellent water-dispersibility. RGD dimer (RGD2, Glu-{Cyclo[Arg-Gly-Asp-(D-Phe)-Lys]}$_2$) and lactoferrin (LF) were then conjugated to ES-GON-rBSA to generate composite nanoparticle ES-GON-rBSA-LF-RGD2 (Figure 1 a). ES-GON-rBSA-FL-RGD2 with extraordinary relaxivities ($r_1 = 60.8$ mM^{-1} s^{-1}, $r_2/r_1 = 1.1$) can transport across the BBB due to its extremely small particle size ($d_h = 13.4$ nm) and LF receptor mediated transcytosis, can be internalized into brain tumor cells due to RGD2 receptor (*i.e.* integrin $\alpha_v\beta_3$) mediated endocytosis, and thus can be used to evaluate and monitor radiosensitization of brain tumors *via* high contrast MRI (Figure 1 b).

2. Materials and methods

2.1. Synthesis of ES-GON-rBSA

ES-GON was first synthesized by a wet-chemical method. Typically, the oxygen in PAA solution (4.0 mg/mL, 200 mL, Mw = 1.8 kDa) in three-necked round bottom flask was removed *via* nigrogen bubbling for around 50 min. The three-necked round bottom flask was then put in 100 °C of oil bath to reflux. After that, Gd(NO$_3$)$_3$ (125 mM, 4.0 mL) and NH$_3$·H$_2$O (28 %, 30 mL) were respectively injected into the PAA solution. ES-GON was obtained after 60 min of reaction. The ES-GON sample was purified *via* dialysis (Mw cut-off 6–8 kDa), concentrated *via* rotary evaporation, and its Gd concentration was determined *via* inductively coupled plasma optical emission spectrometry (ICP-OES; Agilent 5100).

20 mg NaBH$_4$ was added into 20 mg/mL of BSA (40 mL) under magnetic stirring. After 2.0 h of reaction, reductive BSA (rBSA) was obtained. After that, EDC (10 μL, 55 μmol) and NHS (17.4~174 μL, 13 mg/mL, 2.0~20 μmol) were mixed with ES-GON solution (3.0 mL, $C_{Gd} = 3.12$ mM, ice cold) under magnetic stirring. After 5 min, 98.3~983 μL of rBSA (20 mg/mL) was added, and the solution volume was tuned to 5.0 mL using pure water. After 16 h of reaction, the rBSA-stabilized ES-GON (ES-GON-rBSA) solutions were obtained.

2.2. Synthesis of ES-GON-rBSA3-LF-RGD2

The LF and RGD2 were grafted to the surface of ES-GON-rBSA3 by the reaction between –COOH and –NH$_2$. Briefly, EDC (10 μL, 55 μmol) and NHS (50 μL, 13 mg/mL, 5.65 μmol) were mixed with ES-GON-rBSA3 solution (5.0 mL, C_{Gd} = 1.87 mM) under stirring. LF (10 mg/mL, 200 μL, 0.125 mM) and RGD2 (5.0 mg/mL, 100 μL, 3.8 mM) were then charged to the above solution. After 16 h, the obtained ES-GON-rBSA3-LF-RGD2 was rinsed 3 times utilizing pure water *via* ultrafiltration (molecular size cutoff of 10 kDa). The final sample was dispersed in 5.0 mL of pure water.

2.3. Preparation of R6G-ES-GON-rBSA3 or R6G-ES-GON-rBSA3-LF-RGD2

To study the cellular uptake of ES-GON-rBSA3 or ES-GON-rBSA3-LF-RGD2 using flow cytometry or laser scanning confocal microscopy (LSCM), Rhodamine 6G (R6G) was loaded using ES-GON-rBSA3 or ES-GON-rBSA3-LF-RGD2. Briefly, R6G (0.7 mL, 10 μM) was added into ES-GON-rBSA3 (4.0 mL, C_{Gd}=1.87 mM), or ES-GON-rBSA3-LF-RGD2 (4.0 mL, C_{Gd}=1.87 mM), and stirred 24 h at room temperature. After that, the unloaded R6G was removed by rinsing R6G-ES-GON-rBSA3 and R6G-ES-GON-rBSA3-LF-RGD2 solutions utilizing pure water *via* ultrafiltration (Mw cut-off 10 kDa). The final samples of R6G-ES-GON-rBSA3 and R6G-ES-GON-rBSA3-LF-RGD2 were dissolved in pure water (4.0 mL) for next use.

3. Results and Discussion

3.1. Synthesis and characterization of ES-GON-rBSA-LF-RGD2

ES-GON-rBSA1–4 nanoparticles were synthesized with various feeding amounts of rBSA. The r_1 and r_2 of ES-GON-rBSA1–4 were first measured on a 7.0 T MRI scanner system (Figure S1, Table S1). With decreasing feeding amount of rBSA, the r_1 increased and the r_2/r_1 decreased. That's because the excessive conjugation of rBSA decreases the interaction between the H$_2$O molecules and the naked Gd on the surface of ES-GON-rBSA. ES-GON-rBSA3 was chosen as an optimal one due to its relatively high r_1, low r_2/r_1, and high rBSA content.

The number of Gd$_2$O$_3$ in each ES-GON nanoparticle (N_{Gd2O3}) can be calculated according to the following equation (1):

$$N_{Gd_2O_3} = \frac{\rho \times \frac{4}{3}\pi r^3}{Mw} \times 6.02 \times 10^{23} \tag{1}$$

where ρ is the density of Gd$_2$O$_3$ (7.41 g/cm^3), r is the radius of the ES-GON (0.95 nm), and M$_w$ is the molecular weight of Gd$_2$O$_3$ (362.5 g/mol). According to the Eq. (1), the N_{Gd2O3} of ES-GON nanoparticle is calculated to be 44.2. The average number ratio of RGD2 and LF molecule to ES-GON nanoparticle (*i.e.*, NR$_{RGD2/ES-GON}$ and NR$_{LF/ES-GON}$) was then calculated to be 3.6 and 0.23, respectively. In addition, the average NR$_{rBSA/ES-GON}$ was calculated to be 1.5, 1.1, 0.6, and 0.2 for ES-GON-rBSA1–4 (Table S1). 0.2 of NR$_{rBSA/ES-GON}$ mean that five ES-GON was conjugated to one rBSA. Which is reasonable

because rBSA is a macromolecule (Mw = 66.5 kDa) and the ES-GON is extremely small (< 2.0 nm).

To meet the criteria of theranostic application for glioblastoma, RGD2 and LF were conjugated to ES-GON-rBSA3 to generate composite nanoparticle ES-GON-rBSA3-LF-RGD2 (Figure 1). The LF receptor mediated transcytosis can help ES-GON-rBSA3-LF-RGD2 transport across the BBB,[17–20] and the interaction between integrin $\alpha_v\beta_3$ and RGD2 can help ES-GON-rBSA3-LF-RGD2 target brain tumors. The $\alpha_v\beta_3$ integrins are overexpressed on the surface of brain tumor cells and angiogenic endothelial cells, but not (or weakly) expressed in normal tissue and cells, including vascular endothelial cells.[21–23]

Measured on a 7.0 T MRI scanner system, ES-GON-rBSA3-LF-RGD2 has a comparable r_1 value (15.1 mM^{-1} s^{-1}) and r_2/r_1 ratio (3.9) to ES-GON-rBSA3, whose r_1 value is 18.6 mM^{-1} s^{-1} and r_2/r_1 ratio is 3.4 (Figure S1, Table 1). Figure S2 shows T_1-weighted MR images and SNR of the MR images for ES-GON-rBSA3 and ES-GON-rBSA3-LF-RGD2 with various Gd concentrations from 6.25 to 200 μM measured on 7.0 T, which reconfirm the similar MRI efficiency for ES-GON-rBSA3 and ES-GON-rBSA3-LF-RGD2.

Measured on a clinical MRI scanner systems (1.5 T), the r_1 is respectively 64.5 and 60.8 mM^{-1} s^{-1}, and the r_2/r_1 is respectively 1.2 and 1.1 for ES-GON-rBSA3 and ES-GON-rBSA3-LF-RGD2 (Figure 2, Table 1). Although ES-GON-rBSA3-LF-RGD2 has a lower r_1 than that of the ES-GON-rBSA3, the r_1 of ES-GON-rBSA3-LF-RGD2 (60.8 mM^{-1} s^{-1}) is still much higher than the commercial Gd chelates (~ 4 mM^{-1} s^{-1}) and reported Gd-based nanoparticles (4.4 – 47.2 mM^{-1} s^{-1}).[24–31] The r_2/r_1 of ES-GON-rBSA3-LF-RGD2 (1.1) is comparable to the commercial Gd chelates (~ 1.1) and lower than the reported Gd-based nanoparticles (1.1 – 6.8).[24–31] The r_1 and r_2 changed with modifications of LF and RGD2 because the conjugation reaction decreases the interaction between the H$_2$O molecules and the naked Gd on the surface of ES-GON-rBSA.

TEM images (Figure 3 a, b) show that ES-GON-rBSA3 and ES-GON-rBSA3-LF-RGD2 are well-dispersed even at dry state. Figure 3 c shows the size distributions of ES-GON-rBSA3 and ES-GON-rBSA3-LF-RGD2 determined by DLS, and the hydrodynamic sizes (d_h) were measured to be 7.8 and 13.4 nm, respectively. The zeta potentials was measured (Figure 3 d) to be −22.5 mV and −15.2 mV for ES-GON-rBSA3 and ES-GON-rBSA3-LF-RGD2, respectively. The increased d_h and zeta potential indicate the successful conjugation of LF and RGD2 on the surface of ES-GON-rBSA. In addition, the larger hydrodynamic size and negative surface charge of ES-GON-rBSA3-LF-RGD2 assures the longer blood circulation time. In addition, although the hydrodynamic size of ES-GON-rBSA3-LF-RGD2 is up to 13.4 nm, the solid particle size at dry state is < 5 nm (Figure 3 b). Both the small particle size and LF receptor mediated transcytosis facilitate transporting across BBB. The ES-GON-rBSA3-LF-RGD2, featuring extraordinary relaxivities (r_1 = 60.8 mM^{-1} s^{-1}, r_2/r_1 = 1.1), long blood circulation time, and BBB transportability, is very promising for MRI-guided radiosensitization of brain tumors.

The thermogravimetry (TG) and differential thermogravimetry (DTG) curves (Figure S3) show that the weight loss at 1000 °C could be more than 85 % for ES-GON-rBSA3-LF-

RGD2, which indicates the successful conjugation of organic molecules (*i.e.*, rBSA3, LF, and RGD2). In addition, the saturation magnetization (Ms) of ES-GON-rBSA3-LF-RGD2 was determined to be 0.08 emu/g at 30 kOe from the field-dependent magnetization curve (H - M) at 300 K (Figure S4). The low Ms also contributes to the very low r_2/r_1 of ES-GON-rBSA3-LF-RGD2.

Figure S5 a shows that the hydrodynamic sizes of ES-GON-rBSA3-LF-RGD2 (C_{Gd} = 200 μM) after storage in PBS (pH 7.4) or bovine serum albumin (BSA, 10 mg/mL) for 0, 15, or 30 days are similar to those in water. Figure S5 b show that the T_1-weighted MR images of ES-GON-rBSA3-LF-RGD2 (C_{Gd} = 200 μM) after storage BSA (10 mg/mL) for 30 days are also similar to those in water, which were confirmed by the calculated SNR values (Figure S5 c). The long-term storage of ES-GON-rBSA3-LF-RGD2 in PBS or serum did not deteriorate their monodispersity and did not decrease their MR imaging performance, which indicates that our ES-GON-rBSA3-LF-RGD2 has a good stability.

3.2. Cellular uptake of ES-GON-rBSA-LF-RGD2

To investigate the internalization of ES-GON-rBSA3 or ES-GON-rBSA3-LF-RGD2 in cells, Rhodamine 6G (R6G) was loaded *via* ionic, hydrogen and/or coordination bonding to construct R6G-ES-GON-rBSA3 or R6G-ES-GON-rBSA3-LF-RGD2. Figure 4, S7 show the laser scanning confocal microscopy (LSCM) images of U-87 MG or MCF-7 cells after incubation with R6G-ES-GON-rBSA3 or R6G-ES-GON-rBSA3-LF-RGD2 without or with free RGD2 blocking. Figure S6 a summarizes the merged LSCM images. Abundant R6G-ES-GON-rBSA3-LF-RGD2 nanoparticles and very few R6G-ES-GON-rBSA3 nanoparticles were found in the U-87 MG cells (integrin $a_v\beta_3$ positive)[21–23] due to the active targeting function of RGD2. However, almost no R6G-ES-GON-rBSA3-LF-RGD2 nanoparticles were internalized into the U-87 MG cells in the blocking study. Very few R6G-ES-GON-rBSA3-LF-RGD2 and R6G-ES-GON-rBSA3 nanoparticles were found in the MCF-7 cells because the MCF-7 cells are integrin $a_v\beta_3$ negative.[32,33] The red fluorescence signals of R6G in the positive group of Figure S6 a looks weak because the red signal is merged with the blue and green signals. Figure 4 shows the red signal without merging with blue and green signals, which looks much stronger.

The flow cytometry results show that the relative intensity of R6G-ES-GON-rBSA3-LF-RGD2 in U-87 MG cells is much stronger than that of R6G-ES-GON-rBSA3-LF-RGD2 in MCF-7 cells, and R6G-ES-GON-rBSA3 in U-87 MG cells (** P< 0.01) (Figure S8 a–c). Internalized Gd levels in U-87 MG cells measured by ICP are respectively 882 ± 164 and 274 ± 35 fg/cell for ES-GON-rBSA3-LF-RGD2 and ES-GON-rBSA3 (Figure S8 d). However, in the presence of 200 times of free RGD2 blocking, it is only 386 ± 42 fg/cell for ES-GON-rBSA3-LF-RGD2 (*** P< 0.001) (Figure S8 d). These results reinforce that ES-GON-rBSA3-LF-RGD2 can be internalized into brain tumor cells due to RGD2 receptor (*i.e.* integrin $a_v\beta_3$) mediated endocytosis.

Figure S9 shows LSCM images of U-87 MG cells after incubation with R6G-ES-GON-rBSA3-LF-RGD2 nanoparticles. Some nucleus positions are pointed out using solid white circles, and some endosome or lysosome positions are indicated using dotted white circles. The red nanoparticles overlap with green endosome (or lysosome) and blue nucleus, which

demonstrates that the nanoparticles were internalized into endosomes *via* endocytosis mechanism, and some of them escaped from the endosome and lysosome and entered into the nucleus.

3.3. MR imaging of cells and cytotoxicity of ES-GON-rBSA-LF-RGD2

Figure S10 a, b shows the T_1-weighted MR images of U-87 MG cells. The MRI signal of ES-GON-rBSA3-LF-RGD2 looks much stronger than that of the Magnevist and the Control untreated with contrast agents. The SNR of the MR images is respectively 275 % and 89 % for ES-GON-rBSA3-LF-RGD2 and Magnevist (Figure S10 c). The significant differences (* $P < 0.05$) demonstrate the outstanding MRI efficiency of ES-GON-rBSA3-LF-RGD2.

The results of MTT assay indicate that the cytotoxicity of ES-GON-rBSA3-LF-RGD2 is lower than Magnevist on U-87 MG cells or MCF-7 cells (* $P < 0.05$, Figure S11 a, b). The lower cytotoxicity of ES-GON-rBSA3-LF-RGD2 can be ascribed from the following three aspects: 1) the Gd_2O_3 is more biocompatible than Gd^{3+}.[24,25,29] 2) the Gd^{3+} in ES-GON-rBSA3-LF-RGD2 nanoparticles is very difficult to be released even in lysosomes (pH 4.5 ~ 5.5) due to the stabilization by PAA and rBSA (Figure S11 c). The Gd^{3+} can be chelated with –COOH from PAA and rBSA, and –NH_2 from rBSA forming Gd-chelates.[34] 3) The different cytotoxicity between nanoparticles and Magnevist may be caused by their different cell uptake behavior. The small molecular such as Gd-chelates is easy to enter into cells.

3.4. ES-GON-rBSA-LF-RGD2-mediated radiosensitization of cancer cells

Due to the high atomic mass (Z = 64), gadolinium-based nanoparticles hold potential to serve as radiosensitizing agents to enhance the radiation therapy effects.[35–37] ES-GON and ES-GON-rBSA3-LF-RGD2-mediated radiosensitization of cancer cells was quantified by a clonogenic assay. Figure S6 b shows the survival fraction of U-87 MG cells irradiated by 212 kVp X-rays between 0 and 8 Gy *in vitro*. It's obvious that the cells incubated with ES-GON-rBSA3 or ES-GON-rBSA3-LF-RGD2 nanoparticles are more sensitive to the X-ray radiation than the control cells (untreated with nanoparticles). Regression analysis was utilized to fit the data to a linear-quadratic model:[35]

$$\log[\text{Survival Fraction}] = \alpha \times [dose] + \beta \times [dose]^2 \tag{2}$$

According to the fitting formulas (Figure S6 b), the X-ray dose with 50 % of survival fraction (D_{SF50}) was respectively calculated to be 2.69, 1.95, and 1.78 Gy for the control (without nanoparticles), ES-GON-rBSA3, and ES-GON-rBSA3-LF-RGD2. According to equation (3),[37] the sensitivity enhancing factor (EF) was respectively calculated to be 27.5 % and 33.8 % for ES-GON-rBSA3 and ES-GON-rBSA3-LF-RGD2, which are slightly lower than gold NPs/clusters[35] because the atomic number of Gd (Z = 64) is lower than gold (Z = 79).

$$\text{EF (\%)} = \frac{D_{SF50} \, of \, Control - D_{SF50} \, of \, Nanoparticles}{D_{SF50} \, of \, Control} \times 100\% \tag{3}$$

These results indicate that ES-GON-rBSA3 and ES-GON-rBSA3-LF-RGD2 could be used as effective radiosensitizing agents to enhance the radiation therapy effects.

To study the radiosensitizing mechanism of our nanoparticles, the intracellular generation of ROS was determined by a fluorogenic reagent DCF-DA (2,7-dichlorofluorescein diacetate), which could be oxidized to the highly fluorescent DCF (dichlorofluorescein) by ROS. Figure S6 c shows the DCF fluorescence distributions (measured by flow cytometry analysis) of U-87 MG cells incubated with or without ES-GON-rBSA3-LF-RGD2, and irradiated with or without 212 kVp X-ray (4 Gy). As a control, the cells were incubated with NAC (*i.e.*, N-Acetyl-L-cysteine, a ROS scavenger) to remove the intercellular ROS. The relative intensity (Figure S6 d) of the cells incubated with ES-GON-rBSA3-LF-RGD2 and irradiated with X-ray was 3.1 ± 0.4, which is much higher than that of the cells with X-ray irradiation alone (1.7 ± 0.4), or with ES-GON-rBSA3-LF-RGD2 incubation but without X-ray irradiation (1.2 ± 0.3). In addition, pretreatment with NAC decreased the relative intensity from 3.1 ± 0.4 to 1.5 ± 0.3. The intracellular ROS generation and scavenging were also observed by LSCM *via* DCF-DA assay (Figure S12). These results demonstrate that incubation with ES-GON-rBSA3-LF-RGD2 can enhance intracellular generation of ROS under X-ray irradiation, which is the mechanism of radiosensitization.

3.5. BBB transportability of ES-GON-rBSA-LF-RGD2 in vitro and in vivo

The blood-brain barrier (BBB), which is composed of endothelial cells forming a dense layer and connected by tight junctions, can hinder many molecules from penetrating the brain.[38] It is the most formidable barrier of the physiological barriers to overcome for delivery of nanomedicines into the brain.[17,39] In order to demonstrate the feasibility of ES-GON-rBSA3-LF-RGD2 nanoparticles as a theranostic agent for T_1-weighted MR imaging and radiosensitization of glioblastoma, the *in vitro* BBB model was constructed to study the BBB permeability of ES-GON-rBSA3-LF-RGD2 (Figure S13 a). Figure S13 b shows the percentages of ES-GON-rBSA3, ES-GON-rBSA3-RGD2, ES-GON-rBSA3-LF, ES-GON-rBSA3-LF-RGD2, ES-GON-rBSA3-LF-RGD2 plus LF block, or Magnevist in the apical chamber or basolateral chamber of all the feeding nanoparticles. 49.7 ± 2.4 % of Magnevist was found in the basolateral chamber after 12 h indicating the *in vitro* BBB model is not as tight as the real *in vivo* BBB, which exclude most of the polar molecules and small ions.[17] That's because the real *in vivo* BBB, constructing from at least cerebral endothelial cells, basement membrane and astrocyto foot, is much more complicated than the *in vitro* BBB model. Although the *in vitro* BBB model is hard to exclude small molecules, only 15.2 ± 1.0 % of ES-GON-rBSA3, and 14.0 ± 1.3 % of ES-GON-rBSA3-RGD2 were found in the basolateral chamber after 12 h, which demonstrates that the *in vitro* BBB model is tight enough to exclude most of the small ES-GON-rBSA3 and ES-GON-rBSA3-RGD2 nanoparticles. Furthermore, much more ES-GON-rBSA3-LF (33.9 ± 2.1%) and ES-GON-rBSA3-LF-RGD2 (35.6 ± 1.5%) transported across the *in vitro* BBB model, and excessive LF blocking reduced the BBB permeability to only 11.6 ± 0.8 % (# $P < 0.005$). These results demonstrate that LF can be used to mediate BBB transcytosis of nanoparticles.

We investigated the *in vivo* BBB transportability of ES-GON-rBSA3-LF-RGD2 compared with Magnevist. Figure 5 shows the T_1-weighted MR images of normal mouse brains (without tumors) at different slices before or after intravenous injection of Magnevist or ES-GON-rBSA3-LF-RGD2. The Gd dosage is 5.0 mg/kg. The slices with strongest MRI signals at various time points are summarized in Figure S14 a, b. It is clearly observed that ES-

GON-rBSA3-LF-RGD2 can transport across the *in vivo* BBB and reach the brain enhancing MRI contrast of the brain, but Magnevist almost cannot accumulate in brain at this Gd dosage. Figure S14 c, d shows quantitative analysis of the T_1-weighted MR images at different time points showing average SNR calculated from three different slices (from Figure 5). The SNR and SNR were calculated in in accordance with the equation (4) and (5).

$$\text{SNR} = \frac{SI_{mean}}{SD_{noise}} \tag{4}$$

$$\Delta\text{SNR} = \frac{SNR_{post} - SNR_{pre}}{SNR_{pre}} \times 100\% \tag{5}$$

The SNR is only 20 ± 4 % at 1 h post-injection, and reaches a maximum (73 ± 17 %) at 12 h post-injection of ES-GON-rBSA3-LF-RGD2, which is much higher than the maximum of Magnevist ($28 \pm 12\%$ at 10 min post injection). The high SNR in healthy brain demonstrates the *in vivo* BBB transportability of ES-GON-rBSA3-LF-RGD2.

Therefore, ES-GON-rBSA3-LF-RGD2 can transport across the *in vitro* BBB model and the *in vivo* BBB of mice due to LF-mediated transcytosis and the extremely small particle size.

3.6. In vivo MRI-guided radiosensitization of subcutaneous glioblastoma

In order to investigate the T_1-weighted MR imaging efficacy of ES-GON-rBSA3-LF-RGD2 for *in vivo* glioblastoma, a U-87 MG tumor model was inoculated into nude mice, and ES-GON-rBSA3-LF-RGD2 were intravenously injected with T_1-weighted MR images (axial) observed at various times post-injection (Figure S15). It was found that the MRI signals in tumors were very weak before intravenous injection, became stronger after intravenous injection, and attained at maximum at 12 h post-injection for ES-GON-rBSA3-LF-RGD2 (Figure S15 a–e). Figure S15 f show the quantitative analysis of tumors after treatment with ES-GON-rBSA3-LF-RGD2. The SNR increases after intravenous injection and the maximum reaches to 423 ± 42 % at 12 h post-injection of ES-GON-rBSA3-LF-RGD2, which is much higher than that of the reported nanoparticles and Gd-chelates (< 80 %).[40–43] The maximum SNR is only $75 \pm 11\%$ at 20 min post-injection for Magnevist.[44]

We also scanned the T_1 images (coronal) of U-87 MG tumor-bearing nude mice at different slices before or after intravenous injection of ES-GON-rBSA3-LF-RGD2. The slices with strongest tumor or liver MRI signals at different time points are summarized in Figure 6 a, b. It was obvious that the MRI signal in both tumor and liver reaches a maximum at 12 h post-injection of ES-GON-rBSA3-LF-RGD2, and it is stronger in tumor than liver. The signal changes in tumor or liver at different time points are analyzed using SNR, and Figure 6 c, d shows the quantitative analysis results of tumor and liver. The highest SNR at 12 h post-injection is respectively 363 ± 63 %, and 283 ± 52 % for tumor and liver (* $P < 0.05$). The high SNR values result from the extraordinary relaxivities ($r_1 = 60.8$ mM^{-1} s^{-1}, $r_2/r_1 = 1.1$) of ES-GON-rBSA3-LF-RGD2. The higher SNR in tumor *versus* the liver can be attributed

to the higher ES-GON-rBSA3-LF-RGD2 accumulation in tumor due to the small particle size (d_h = 13.4 nm) and RGD2-based active targeting.

We further evaluated the radiosensitization efficacy of ES-GON-rBSA3-LF-RGD2 on subcutaneous glioblastoma. Figure 6 e shows the anti-tumor efficacies of ES-GON-rBSA3-LF-RGD2 on U-87 MG tumor-bearing mice with or without irradiation of X-ray. It is obvious that the tumors grow very fast without X-ray irradiation no matter whether ES-GON-rBSA3-LF-RGD2 is injected or not, which indicates that ES-GON-rBSA3-LF-RGD2 alone is not toxic. However, with X-ray irradiation, the tumor growth could be further inhibited by the ES-GON-rBSA3-LF-RGD2 treatment due to its radiosensitization, which can be ascribed to the high atomic mass of Gd (Z = 64) and generation of ROS. The mouse survival rates of ES-GON-rBSA3-LF-RGD2+X-ray group are much higher than that of ES-GON-rBSA3-LF-RGD2 group. The former is always 100 % in 22 days, but the latter is only 20 % on day 20 and 0 % on day 22 (Figure 6 f). The survival curve of "PBS + X-ray" group in Figure 6 f can be barely seen because it overlaps with the that of the "ES-GON-rBSA3-LF-RGD2 + X-Ray" group. The relative body weights of the mice with ES-GON-rBSA3-LF-RGD2 radiosensitization (*i.e.*, group of ES-GON-rBSA3-LF-RGD2 plus X-Ray irradiation) are larger than the group of PBS plus X-Ray irradiation (Figure 6 g). The use of ES-GON-rBSA3-LF-RGD2 mitigated the weight loss of mice by X-ray irradiation because the tumor growth were well suppressed and the ES-GON-rBSA3-LF-RGD2 radiosensitization reduced the side effects of radiation therapy.

The high ES-GON-rBSA3-LF-RGD2 accumulation in tumor was further confirmed by the evaluation of *in vivo* biodistribution determined by ICP. Figure S16 shows that the Gd levels are all very low (< 0.5 %ID/g of tissue) in heart, liver, spleen, lung, kidney, tumor and brain at 6 days post-injection of ES-GON-rBSA3-LF-RGD2. This result demonstrates that most of ES-GON-rBSA3-LF-RGD2 nanoparticles could be excreted from the body resulting in very low risk of kidney injury caused by Gd. In addition, at 12 h post-injection of ES-GON-rBSA3-LF-RGD2, the Gd levels are < 0.8 %ID/g of tissue in heart, lung, kidney and brain, but they are respectively 4.9 ± 2.4, 5.1 ± 1.9, and 7.3 ± 3.4 %ID/g of tissue in liver, spleen and tumor. These results are consistent with the *in vivo* T_1-weighted MR images (Figure 6 a–d) showing high tumor accumulation of ES-GON-rBSA3-LF-RGD2. The high tumor accumulation, superhigh r_1 value, and ultralow r_2/r_1 ratio of ES-GON-rBSA3-LF-RGD2 lead to low Gd dosage for theranostic application, which also reduces the risk of kidney injury caused by Gd.

3.7. In vivo toxicity studies

Figure S17 presents the histological analyses of major organs from the subcutaneous tumor-bearing nude mouse (control), and that with once or thrice intravenous injection of ES-GON-rBSA3-LF-RGD2 with or without irradiation of X-ray. Comparing with the control, the tumor-bearing nude mouse after once or thrice injection of ES-GON-rBSA3-LF-RGD2 with or without irradiation of X-ray did not exhibit obvious toxicity of the major organs (*i.e.* heart, kidney, liver, lung and spleen), indicating that the biosafety of our radiosensitizing agent is good even after three doses. In addition, ES-GON-rBSA3-LF-RGD2 treatment without irradiation of X-ray did not induce therapeutic efficiency to the tumor, but that with

irradiation of X-ray did result in obvious killing effect of tumor cells. These results reinforce that our radiosensitizing agent ES-GON-rBSA3-LF-RGD2 is biocompatible.

Because the requirement of particle size threshold for renal excretion is considered to be ~ 6 nm,[40,45] Although the hydrodynamic size of ES-GON-rBSA3-LF-RGD2 is a little bit large (d_h = 13.4 nm), the renal excretion is also applicable to it because the solid particle size is < 5 nm (Figure 3 b).

Because the transplantation of orthotopic glioblastoma mouse model is much more challenging than that of ectopic subcutaneous glioblastoma mouse model, the above tests including *in vivo* toxicity and *in vivo* biodistribution of Gd were first performed using the subcutaneous glioblastoma model. Then T_1-weighted MRI and radiosensitization studies were carried out using the orthotopic glioblastoma model (Figure 7, Figure 8, Figure S18, Figure S19).

3.8. T1-weighted MRI of orthotopic brain tumors

Figure 7 a–c shows the T_1 images of orthotopic brain tumor-bearing nude mice. The MRI signal of tumors at different time points after intravenous injection of Magnevist is comparable to that before injection, which indicates that Magnevist cannot enhance the contrast of orthotopic brain tumors due to the BBB. However, at 8 h post injection of ES-GON-rBSA3-LF-RGD2 nanoparticles, the contrast of orthotopic brain tumor was enhanced significantly. The highest SNR of ES-GON-rBSA3-LF-RGD2 nanoparticles is much higher than that of Magnevist and ES-GON-rBSA3-RGD2 nanoparticles without conjugation of LF (Figure S18, *** P < 0.001). These results demonstrate that ES-GON-rBSA3-LF-RGD2 nanoparticles can transport across the *in vivo* BBB and accumulate in the orthotopic brain tumors due to the conjugation of LF and RGD2.

3.9. Radiosensitization of orthotopic glioblastoma models

The orthotopic glioblastoma models were established using U87-Luc and U251-Luc cells according to literatures.[46,47] The treatment efficiency of ES-GON-rBSA3-LF-RGD2 plus radiotherapy on these two orthotopic glioblastoma models with bioluminescence imaging was evaluated on days 2, 7 and 14 after treatment. Significant reduction in bioluminescence signals of glioblastoma after treatment with one dose of ES-GON-rBSA3-LF-RGD2 plus radiotherapy was observed as shown in Figure 8, S19. However, other treatments (controls) cannot reduce the glioblastoma growth. In addition, treatment with ES-GON-rBSA3-LF-RGD2 plus radiotherapy significantly extended mouse survival (Figure 8, S19). The therapeutic studies on orthotopic glioblastoma models reinforce that ES-GON-rBSA3-LF-RGD2 can enhance the radiation therapy of brain tumors as an effective radiosensitizing agent.

4. Conclusions

In summary, BBB-transportable small-sized gadolinium oxide based nanoparticles were developed for high contrast MRI and radiosensitization of orthotopic GBM. ES-GON-rBSA was synthezed in water solutions, resulting in excellent water-dispersibility. RGD2 and LF were then conjugated to the ES-GON-rBSA to generate composite nanoparticle ES-GON-

rBSA-LF-RGD2. Due to the LF-mediated transcytosis and the extremely small particle size ($d_h = 13.4$ nm), ES-GON-rBSA3-LF-RGD2 can transport across the *in vitro* BBB model and the *in vivo* BBB of mice. Because of the integrin $\alpha_v\beta_3$-mediated endocytosis, ES-GON-rBSA3-LF-RGD2 can be internalized into brain tumor cells. The ES-GON-rBSA-FL-RGD2 with extraordinary relaxivities ($r_1 = 60.8$ mM^{-1} s^{-1}, $r_2/r_1 = 1.1$) can be used as a strong T_1-weighted MRI contrast agent, which allows for evaluation and monitoring of tumor therapy. The maximum signal enhancement (SNR) for T_1-weighted MRI of tumors reached up to 423 ± 42 % at 12 h post-injection of ES-GON-rBSA-LF-RGD2, which is much higher than commercial Gd-chelates ($< 80\%$). Based on the nanoparticle-mediated radiosensitization studies on cells, subcutaneous and orthotopic glioblastoma models, we believe that ES-GON-rBSA3-LF-RGD2 nanoparticles are biocompatible, and could be used as effective radiosensitizing agents to enhance the radiation therapy effects based on the mechanism of ROS generation.

Supplementary Material

Refer to Web version on PubMed Central for supplementary material.

Acknowledgements

References

[1]. Gilbert MR, Dignam JJ, Armstrong TS, Wefel JS, Blumenthal DT, Vogelbaum MA, Colman H, Chakravarti A, Pugh S, Won M, Jeraj R, Brown PD, Jaeckle KA, Schiff D, Stieber VW, Brachman DG, Werner-Wasik M, Tremont-Lukats IW, Sulman EP, Aldape KD, Curran WJ Jr., Mehta MP, A Randomized Trial of Bevacizumab for Newly Diagnosed Glioblastoma, N. Engl. J. Med 370 (2014) 699–708. [PubMed: 24552317]

[2]. Chinot OL, Wick W, Mason W, Henriksson R, Saran F, Nishikawa R, Carpentier AF, Hoang-Xuan K, Kavan P, Cernea D, Brandes AA, Hilton M, Abrey L, Cloughesy T, Bevacizumab plus Radiotherapy–Temozolomide for Newly Diagnosed Glioblastoma, N. Engl. J. Med 370 (2014) 709–722. [PubMed: 24552318]

[3]. Tang W, Fan W, Lau J, Deng L, Shen Z, Chen X, Emerging Blood-Brain-Barrier-Crossing Nanotechnology for Highly Efficient Brain Cancer Theranostics, Chem. Soc. Rev 48 (2019) 2967–3014. [PubMed: 31089607]

[4]. Erel-Akbaba G, Carvalho LA, Tian T, Zinter M, Akbaba H, Obeid PJ, Chiocca EA, Weissleder R, Kantarci AG, Tannous BA, Radiation-Induced Targeted Nanoparticle-Based Gene Delivery for Brain Tumor Therapy, ACS Nano 13 (2019) 4028–4040. [PubMed: 30916923]

[5]. Lundy DJ, Lee KJ, Peng IC, Hsu CH, Lin JH, Chen KH, Tien YW, Hsieh PCH, Inducing a Transient Increase in Blood-Brain Barrier Permeability for Improved Liposomal Drug Therapy of Glioblastoma Multiforme, ACS Nano 13 (2019) 97–113. [PubMed: 30532951]

[6]. Taphoorn MJB, Henriksson R, Bottomley A, Cloughesy T, Wick W, Mason WP, Saran F, Nishikawa R, Hilton M, Theodore-Oklota C, Ravelo A, Chinot OL, Health-Related Quality of Life in a Randomized Phase III Study of Bevacizumab, Temozolomide, and Radiotherapy in Newly Diagnosed Glioblastoma, J. Clin. Oncol 33 (2015) 2166–2175. [PubMed: 26014298]

[7]. Furtado D, Bjornmalm M, Ayton S, Bush AI, Kempe K, Caruso F, Overcoming the Blood–Brain Barrier: The Role of Nanomaterials in Treating Neurological Diseases, Adv. Mater 30 (2018) 1801362.

[8]. Xie J, Shen Z, Anraku Y, Kataoka K, Chen X, Nanomaterial-Based Blood-Brain-Barrier (BBB) Crossing Strategies, Biomaterials 224 (2019) 119491. [PubMed: 31546096]

[9]. Johnsen KB, Moos T, Revisiting nanoparticle technology for blood-brain barrier transport: Unfolding at the endothelial gate improves the fate of transferrin receptor-targeted liposomes, J. Control. Release 222 (2016) 32–46. [PubMed: 26658072]

[10]. Cabezon I, Manich G, Martin-Venegas R, Camins A, Pelegri C, Vilaplana J, Trafficking of Gold Nanoparticles Coated with the 8D3 Anti-Transferrin Receptor Antibody at the Mouse Blood-Brain Barrier, Mol. Pharm 12 (2015) 4137–4145. [PubMed: 26440359]

[11]. Rip J, Chen L, Hartman R, van den Heuvel A, Reijerkerk A, van Kregten J, van der Boom B, Appeldoorn C, de Boer M, Maussang D, de Lange EC, Gaillard PJ, Glutathione PEGylated liposomes: pharmacokinetics and delivery of cargo across the blood-brain barrier in rats, J. Drug Targeting 22 (2014) 460–467.

[12]. Wen X, Wang K, Zhao Z, Zhang Y, Sun T, Zhang F, Wu J, Fu Y, Du Y, Zhang L, Sun Y, Liu Y, Ma K, Liu H, Song Y, Brain-targeted delivery of trans-activating transcriptor-conjugated magnetic PLGA/lipid nanoparticles, PloS One 9 (2014) e106652. [PubMed: 25187980]

[13]. Batrakova EV, Gendelman HE, Kabanov AV, Cell-mediated drug delivery, Expert Opin. Drug Deliv 8 (2011) 415–433. [PubMed: 21348773]

[14]. Zheng M, Liu Y, Wang Y, Zhang D, Zou Y, Ruan W, Yin J, Tao W, Park JB, Shi B, ROS-Responsive Polymeric siRNA Nanomedicine Stabilized by Triple Interactions for the Robust Glioblastoma Combinational RNAi Therapy, Adv. Mater (2019) 1903277.

[15]. Jiang Y, Zhang J, Meng F, Zhong Z, Apolipoprotein E Peptide-Directed Chimeric Polymersomes Mediate an Ultrahigh-Efficiency Targeted Protein Therapy for Glioblastoma, ACS Nano 12 (2018) 11070–11079. [PubMed: 30395440]

[16]. Etame AB, Smith CA, Chan WCW, Rutka JT, Design and potential application of PEGylated gold nanoparticles with size-dependent permeation through brain microvasculature, Nanomedicine 7 (2011) 992–1000. [PubMed: 21616168]

[17]. Yu Y, Jiang X, Gong S, Feng L, Zhong Y, Pang Z, The proton permeability of self-assembled polymersomes and their neuroprotection by enhancing a neuroprotective peptide across the blood-brain barrier after modification with lactoferrin, Nanoscale 6 (2014) 3250–3258. [PubMed: 24503971]

[18]. Zhao X, Ting SM, Liu CH, Sun G, Kruzel M, Roy-O'Reilly M, Aronowski J, Neutrophil polarization by IL-27 as a therapeutic target for intracerebral hemorrhage, Nat. Commun 8 (2017) 602. [PubMed: 28928459]

[19]. Shen Z, Liu T, Li Y, Lau J, Yang Z, Fan W, Zhou Z, Shi C, Ke C, Bregadze VI, Mandal SK, Liu Y, Li Z, Xue T, Zhu G, Munasinghe J, Niu G, Wu A, Chen X, Fenton-reaction-acceleratable magnetic nanoparticles for ferroptosis therapy of orthotopic brain tumors, ACS Nano 12 (2018) 11355–11365. [PubMed: 30375848]

[20]. Agrawal M, Ajazuddin DK Tripathi S Saraf S Saraf SG Antimisiaris S Mourtas M Hammarlund-Udenaes A Alexander, Recent advancements in liposomes targeting strategies to cross blood-brain barrier (BBB) for the treatment of Alzheimer's disease, J. Control. Release 260 (2017) 61–77. [PubMed: 28549949]

[21]. Chen H, Zhao L, Fu K, Lin Q, Wen X, Jacobson O, Sun L, Wu H, Zhang X, Guo Z, Lin Q, Chen X, Integrin αvβ3-targeted radionuclide therapy combined with immune checkpoint blockade immunotherapy synergistically enhances anti-tumor efficacy. Theranostics 9 (2019) 7948–7960. [PubMed: 31695808]

[22]. Zhang L, Su H, Wang H, Li Q, Li X, Zhou C, Xu J, Chai Y, Liang X, Xiong L, Zhang C, Tumor Chemo-Radiotherapy with Rod-Shaped and Spherical Gold Nano Probes: Shape and Active Targeting Both Matter. Theranostics 9 (2019) 1893–1908. [PubMed: 31037146]

[23]. Gao X, Yue Q, Liu Y, Fan D, Fan K, Li S, Qian J, Han L, Fang F, Xu F, Geng D, Chen L, Zhou X, Mao Y, Li C, Image-guided chemotherapy with specifically tuned blood brain barrier permeability in glioma margins. Theranostics. 8 (2018): 3126–3137. [PubMed: 29896307]

[24]. Bridot JL, Faure AC, Laurent S, Riviere C, Billotey C, Hiba B, Janier M, Josserand V, Coll JL, Vander Elst L, Muller R, Roux S, Perriat P, Tillement O, Hybrid Gadolinium Oxide Nanoparticles: Multimodal Contrast Agents for In Vivo Imaging, J. Am. Chem. Soc 129 (2007) 5076–5084. [PubMed: 17397154]

[25]. Park JY, Baek MJ, Choi ES, Woo S, Kim JH, Kim TJ, Jung JC, Chae KS, Chang Y, Lee GH, Paramagnetic Ultrasmall Gadolinium Oxide Nanoparticles as Advanced T_1 MRI Contrast Agent: Account for Large Longitudinal Relaxivity, Optimal Particle Diameter, and In Vivo T_1 MR Images, ACS Nano 3 (2009) 3663–3669. [PubMed: 19835389]

[26]. Zhou LJ, Gu ZJ, Liu XX, Yin WY, Tian G, Yan L, Jin S, Ren WL, Xing GM, Li W, Chang XL, Hu ZB, Zhao YL, Size-Tunable Synthesis of Lanthanide-Doped Gd_2O_3 Nanoparticles and Their Applications for Optical and Magnetic Resonance Imaging, J. Mater. Chem 22 (2012) 966–974.

[27]. Faucher L, Tremblay M, Lagueux J, Gossuin Y, Fortin MA, Rapid Synthesis of PEGylated Ultrasmall Gadolinium Oxide Nanoparticles for Cell Labeling and Tracking with MRI, ACS Appl. Mater. Interfaces 4 (2012) 4506–4515. [PubMed: 22834680]

[28]. Xu W, Park JY, Kattel K, Bony BA, Heo WC, Jin S, Park JW, Chang Y, Do JY, Chae KS, Kim TJ, Park JA, Kwak YW, Lee GH, A T_1, T_2 Magnetic Resonance Imaging (MRI)-Fluorescent Imaging (FI) by Using Ultrasmall Mixed Gadolinium-Europium Oxide Nanoparticles, New J. Chem 36 (2012) 2361–2367.

[29]. Ma XH, Gong A, Xiang LC, Chen TX, Gao YX, Liang XJ, Shen ZY, Wu AG, Biocompatible Composite Nanoparticles with Large Longitudinal Relaxivity for Targeted Imaging and Early Diagnosis of Cancer, J. Mater. Chem. B 1 (2013) 3419–3428.

[30]. Satpathy M, Wang L, Zielinski RJ, Qian W, Wang YA, Mohs AM, Kairdolf BA, Ji X, Capala J, Lipowska M, Nie S, Mao H, Yang L, Targeted Drug Delivery and Image-Guided Therapy of Heterogeneous Ovarian Cancer Using HER2-Targeted Theranostic Nanoparticles. Theranostics 9 (2019) 778–795. [PubMed: 30809308]

[31]. Ray S, Li Z, Hsu CH, Hwang LP, Lin YC, Chou PT, Lin YY, Dendrimer- and copolymer-based nanoparticles for magnetic resonance cancer theranostics. Theranostics 8 (2018) 6322–6349. [PubMed: 30613300]

[32]. Zhang Z, Luo Q, Yan X, Li Z, Luo Y, Yang L, Zhang B, Chen H, Wang Q, Integrin-Targeted Trifunctional Probe for Cancer Cells: a "Seeing and Counting" Approach, Anal. Chem 84 (2012) 8946–8951. [PubMed: 23075036]

[33]. Cao Q, Cai W, Li T, Yang Y, Chen K, Xing L, Chen X, Combination of Integrin siRNA and Irradiation for Breast Cancer Therapy, Biochem. Biophys. Res. Commun 351 (2006) 726–732.

[34]. Shen Z, Wu A, Chen X, Iron Oxide Nanoparticle Based Contrast Agents for Magnetic Resonance Imaging, Mol. Pharm 14 (2017) 1352–1364. [PubMed: 27776215]

[35]. Luchette M, Korideck H, Makrigiorgos M, Tillement O, Berbeco R, Radiation Dose Enhancement of Gadolinium-Based AGuIX Nanoparticles on HeLa Cells, Nanomedicine 10 (2014) 1751–1755. [PubMed: 24941464]

[36]. Song G, Chao Y, Chen Y, Liang C, Yi X, Yang G, Yang K, Cheng L, Zhang Q, Liu Z, All-in-One Theranostic Nanoplatform Based on Hollow TaOx for Chelator-Free Labeling Imaging, Drug Delivery, and Synergistically Enhanced Radiotherapy, Adv. Funct. Mater 26 (2016) 8243–8254.

[37]. Porcel E, Tillement O, Lux F, Mowat P, Usami N, Kobayashi K, Furusawa Y, Le Sech C, Li S, Lacombe S, Gadolinium-Based Nanoparticles to Improve the Hadron Therapy Performances, Nanomedicine 10 (2014) 1601–1608. [PubMed: 24846523]

[38]. Kievit FM, Zhang M, Cancer Nanotheranostics: Improving Imaging and Therapy by Targeted Delivery Across Biological Barriers, Adv. Mater 23 (2011) H217–H247. [PubMed: 21842473]

[39]. Aparicio-Blanco J, Martín-Sabroso C, Torres-Suarez AI, In vitro screening of nanomedicines through the blood brain barrier: A critical review, Biomaterials 103 (2016) 229–255. [PubMed: 27392291]

[40]. Shen Z, Chen T, Ma X, Ren W, Zhou Z, Zhu G, Zhang A, Liu Y, Song J, Li Z, Ruan H, Fan W, Lin L, Munasinghe J, Chen X, Wu A, Multifunctional Theranostic Nanoparticles Based on Exceedingly Small Magnetic Iron Oxide Nanoparticles for T_1-Weighted Magnetic Resonance Imaging and Chemotherapy, ACS Nano 11 (2017) 10992–11004. [PubMed: 29039917]

[41]. Zhang H, Li L, Liu XL, Jiao J, Ng CT, Yi JB, Luo YE, Bay BH, Zhao LY, Peng ML, Gu N, Fan HM, Ultrasmall Ferrite Nanoparticles Synthesized via Dynamic Simultaneous Thermal Decomposition for High-Performance and Multifunctional T_1 Magnetic Resonance Imaging Contrast Agent, ACS Nano 11 (2017) 3614–3631. [PubMed: 28371584]

[42]. Zhou Z, Wu C, Liu H, Zhu X, Zhao Z, Wang L, Xu Y, Ai H, Gao J, Surface and Interfacial Engineering of Iron Oxide Nanoplates for Highly Efficient Magnetic Resonance Angiography, ACS Nano 9 (2015) 3012–3022. [PubMed: 25670480]

[43]. Zhou Z, Wang L, Chi X, Bao J, Yang L, Zhao W, Chen Z, Wang X, Chen X, Gao J, Engineered Iron-Oxide-Based Nanoparticles as Enhanced T_1 Contrast Agents for Efficient Tumor Imaging, ACS Nano 7 (2013) 3287–3296. [PubMed: 23473444]

[44]. Shen Z, Song J, Zhou Z, Yung BC, Aronova MA, Li Y, Dai Y, Fan W, Liu Y, Li Z, Ruan H, Leapman RD, Lin L, Niu G, Chen X, Wu A, Dotted Core-Shell Nanoparticles for T_1-Weighted MRI of Tumors, Adv. Mater 30 (2018) 1803163.

[45]. Liu F, He X, Chen H, Zhang J, Zhang H, Wang Z, Gram-Scale Synthesis of Coordination Polymer Nanodots with Renal Clearance Properties for Cancer Theranostic Applications, Nat. Commun 6 (2015) 8003. [PubMed: 26245151]

[46]. Jin F, Zhao L, Zhao HY, Guo SG, Feng J, Jiang XB, Zhang SL, Wei YJ, Fu R, Zhao JS, Comparison Between Cells and Cancer Stem-Like Cells Isolated from Glioblastoma and Astrocytoma on Expression of Anti-Apoptotic and Multidrug Resistance-Associated Protein Genes, Neuroscience 154 (2008) 541–550. [PubMed: 18462887]

[47]. Jin F, Gao C, Zhao L, Zhang H, Wang HT, Shao T, Zhang SL, Wei YJ, Jiang XB, Zhou YP, Zhao HY, Using CD133 Positive U251 Glioblastoma Stem Cells to Establish Nude Mice Model of Transplanted Tumor, Brain Res 1368 (2011) 82–90. [PubMed: 20971095]
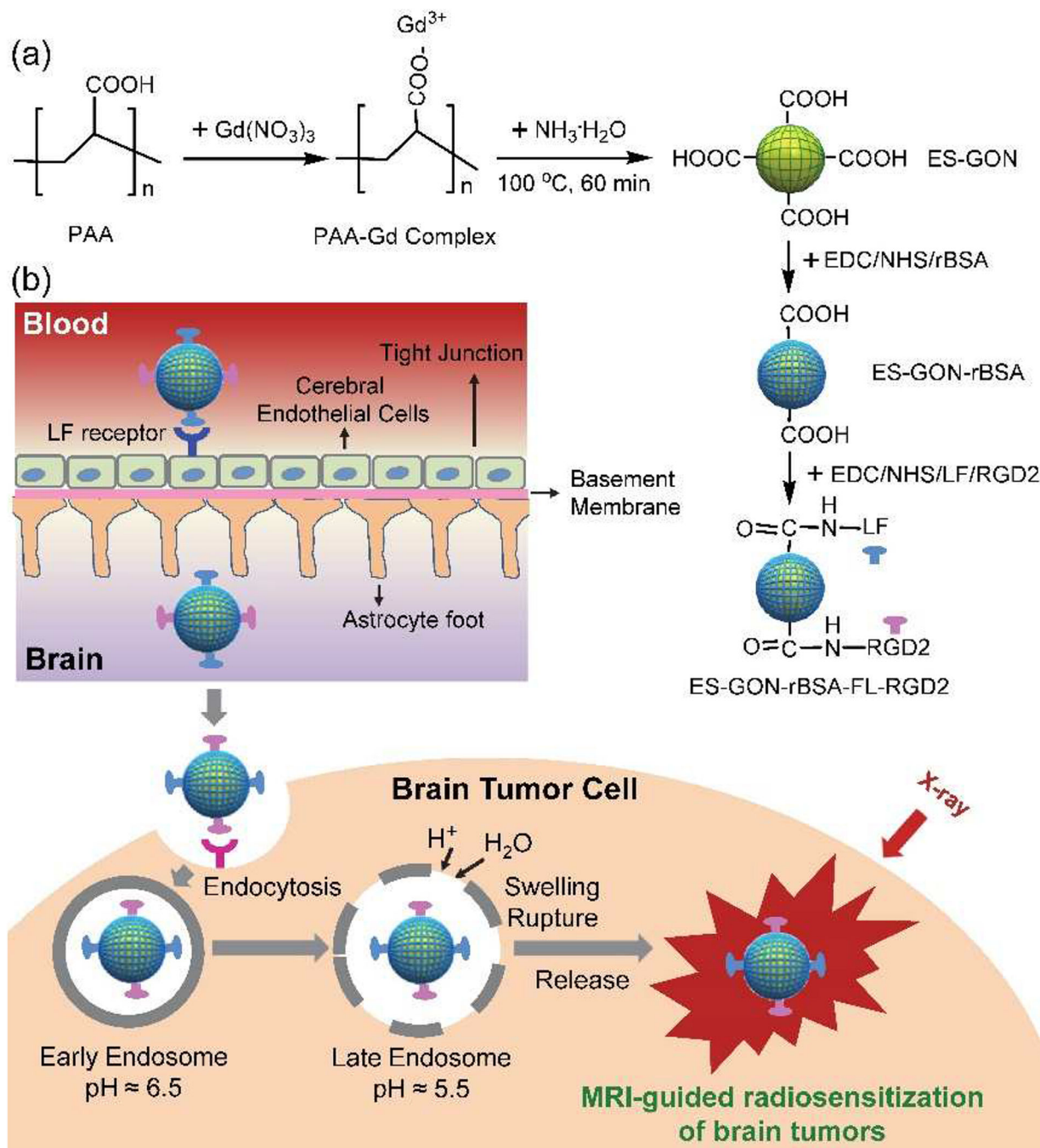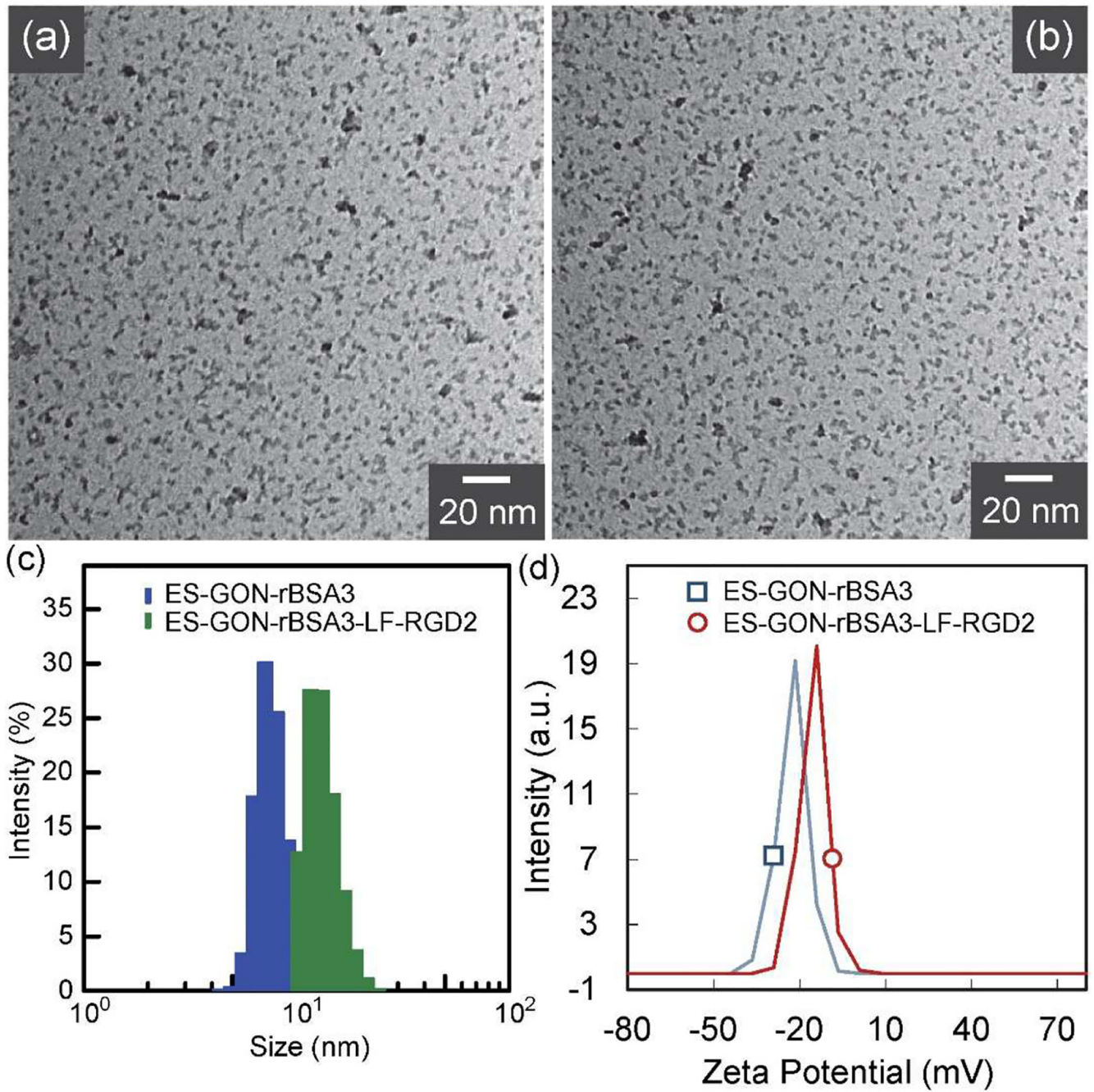
Figure 1.
Scheme for the synthesis of our ES-GON-rBSA and ES-GON-rBSA-FL-RGD2 (a), and the mechanism of MRI-guided radiosensitization of brain tumors (b). The ES-GON-rBSA-FL-RGD2 with extraordinary relaxivities ($r_1 = 60.8$ mM^{-1}1 s^{-1}, $r_2/r_1 = 1.1$) can transport across the BBB due to its extremely small particle size and LF receptor mediated transcytosis, can be internalized into brain tumor cells due to RGD2 receptor (*i.e.* integrin $\alpha_v\beta_3$) mediated endocytosis, and thus can be used for MRI-guided radiosensitization of brain tumors.
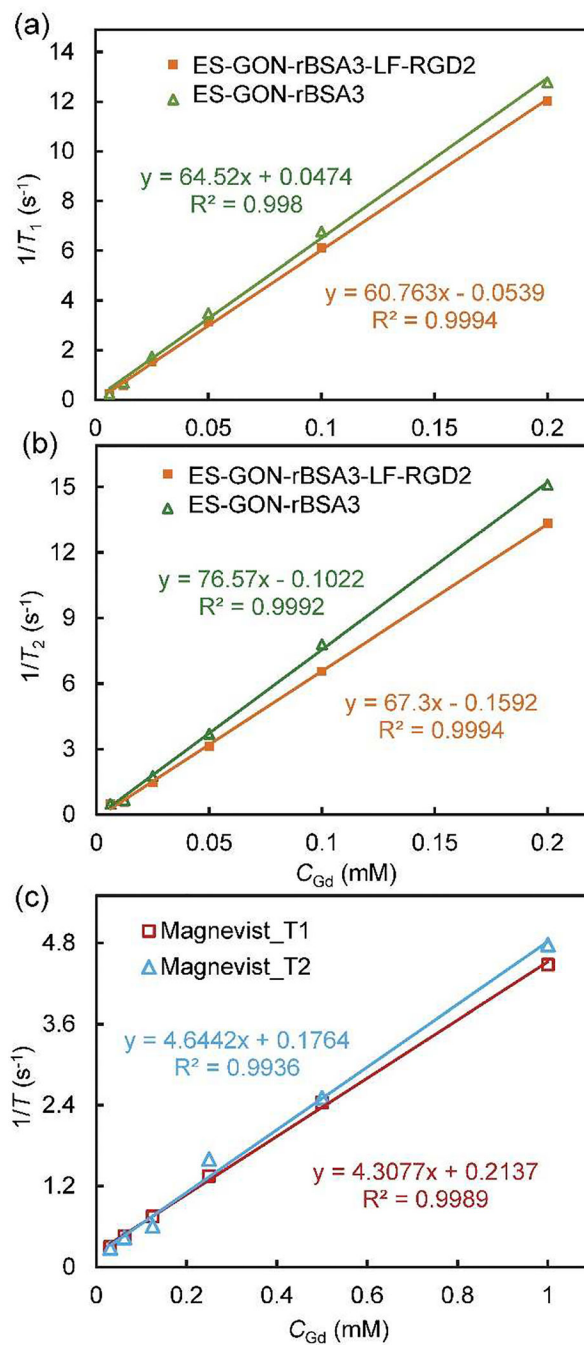
Figure 2.
(a, b): T_1 relaxation rate ($1/T_1$) (a) or T_2 relaxation rate ($1/T_2$) (b) plotted as a function of C_{Gd} for ES-GON-rBSA3, or ES-GON-rBSA3-LF-RGD2. (c): $1/T_1$ or $1/T_2$ plotted as a function of C_{Gd} for Magnevist®. The magnetic field is 1.5 T.

Figure 3.
(a, b): TEM images of ES-GON-rBSA3 (a), and ES-GON-rBSA3-LF-RGD2 (b). (c): Size distribution of ES-GON-rBSA3 ($d_h = 7.8$ nm), and ES-GON-rBSA3-LF-RGD2 ($d_h = 13.4$ nm) determined by DLS. (d): Zeta potential measurement of ES-GON-rBSA3 (−22.5 mV), and ES-GON-rBSA3-LF-RGD2 (−15.2 mV).
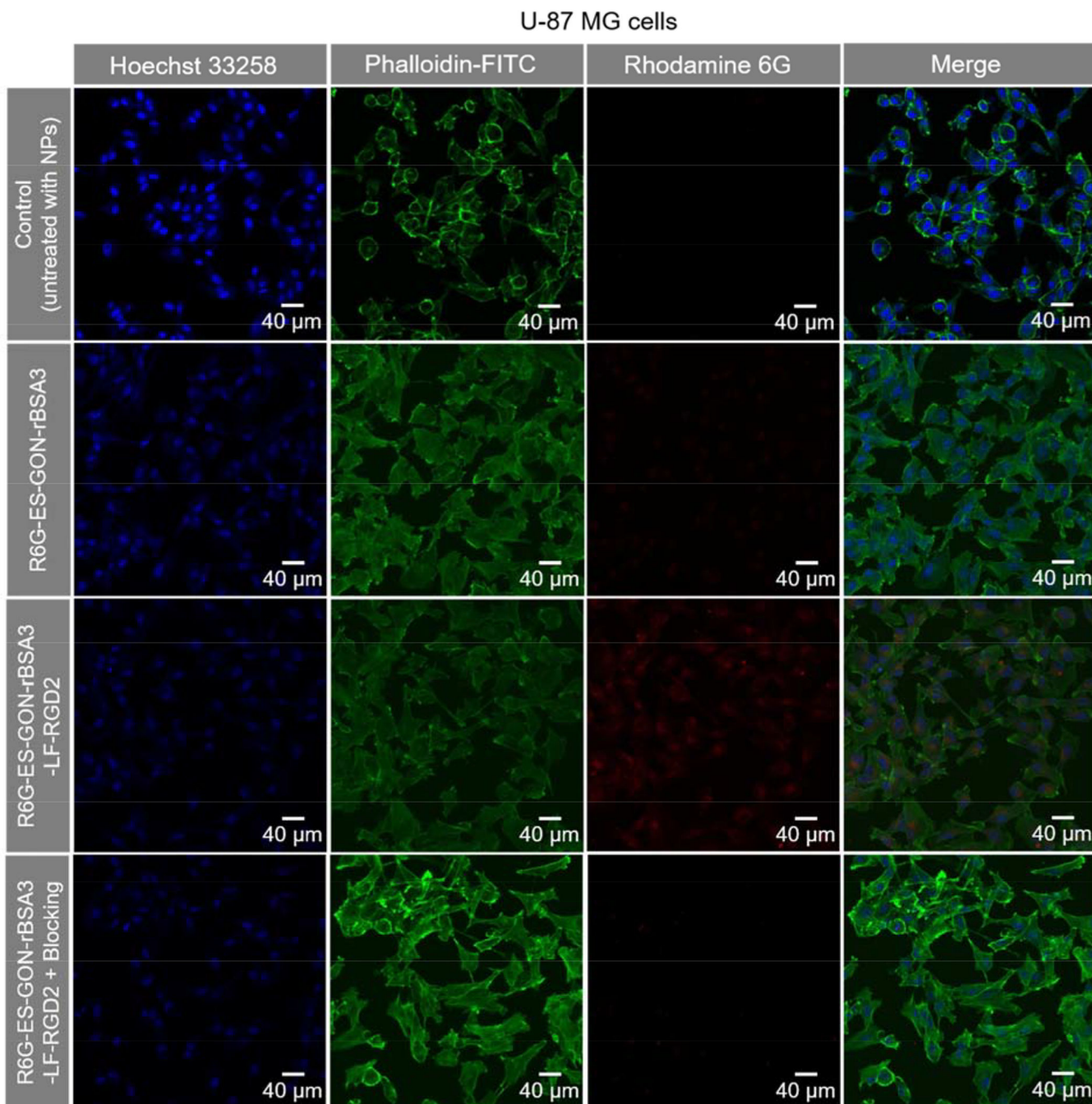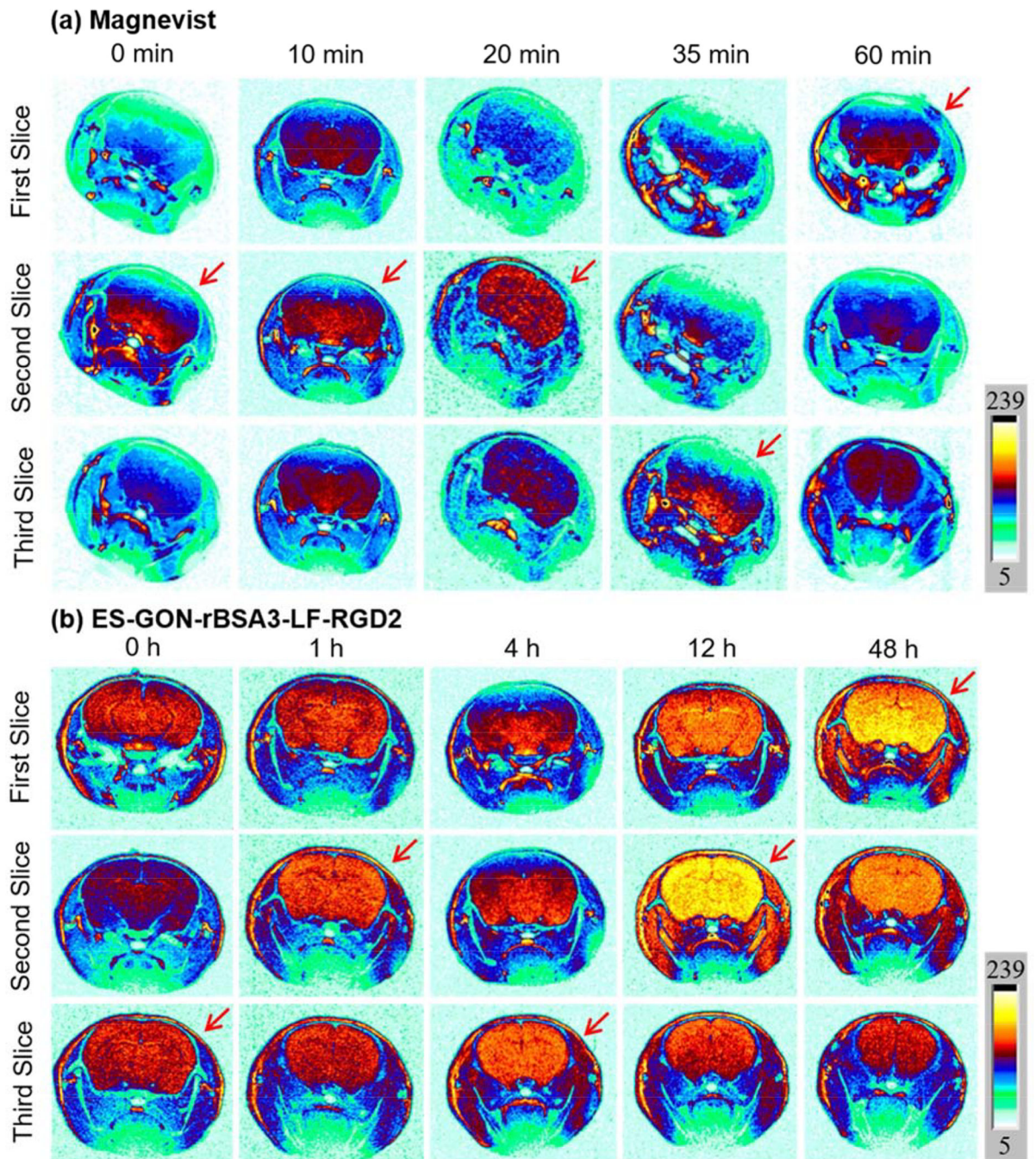
Figure 4.
LSCM images of U-87 MG cells incubated with R6G-ES-GON-rBSA3 or R6G-ES-GON-rBSA3-LF-RGD2 without or with free RGD2 blocking. The blocking study was conducted in the presence of 200 times of free RGD2. The cells untreated with nanoparticles are used as the control. The nucleus stained with Hoechst 33258 is blue, and the cytoskeleton stained with phalloidin-FITC is green. The R6G-loaded nanoparticles are red.
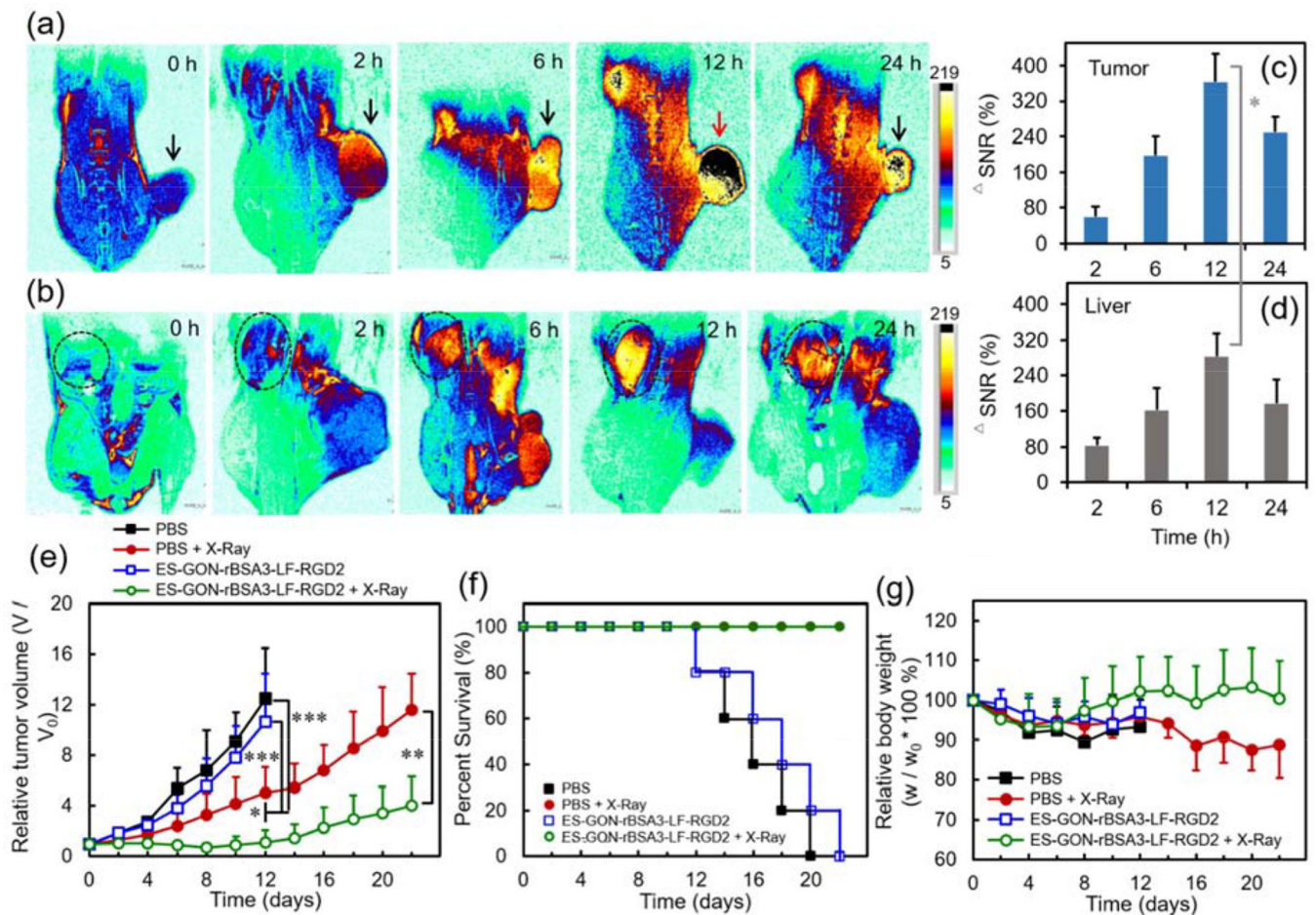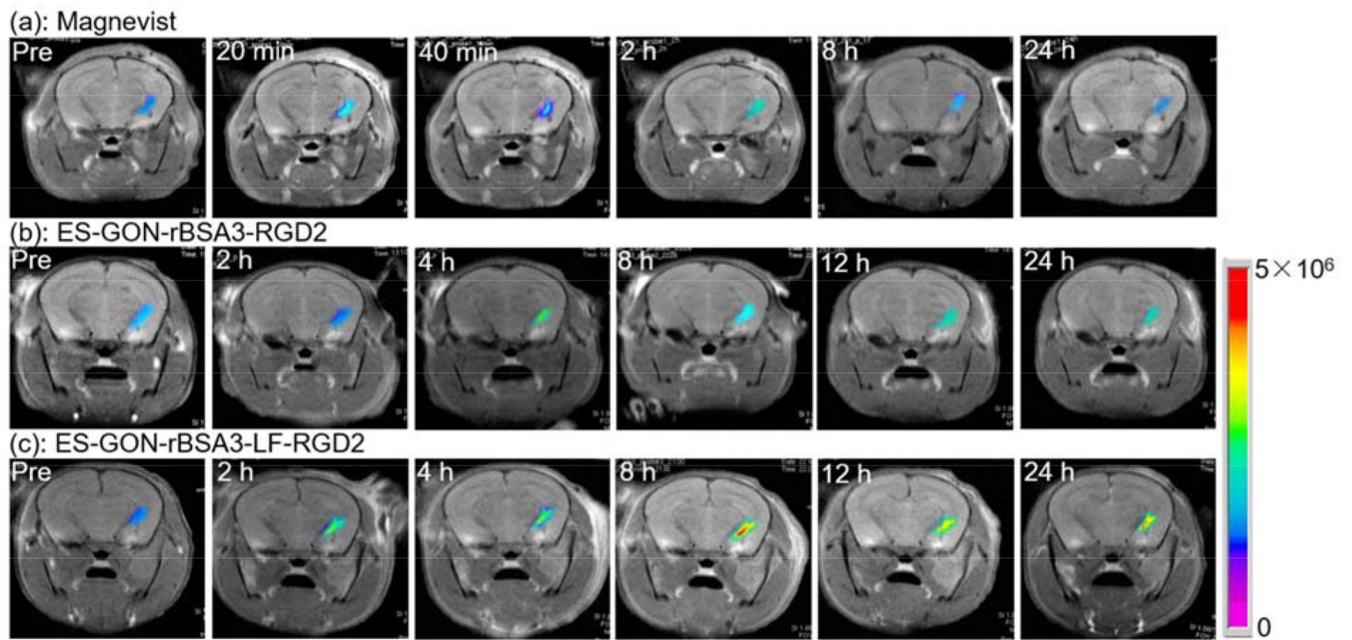
Figure 5.
T_1-weighted MRI images of healthy mouse brains at different slices pre or post i.v. injection of Magnevist (a), or ES-GON-rBSA3-LF-RGD2 (b). Gd dose = 5.0 mg/kg.
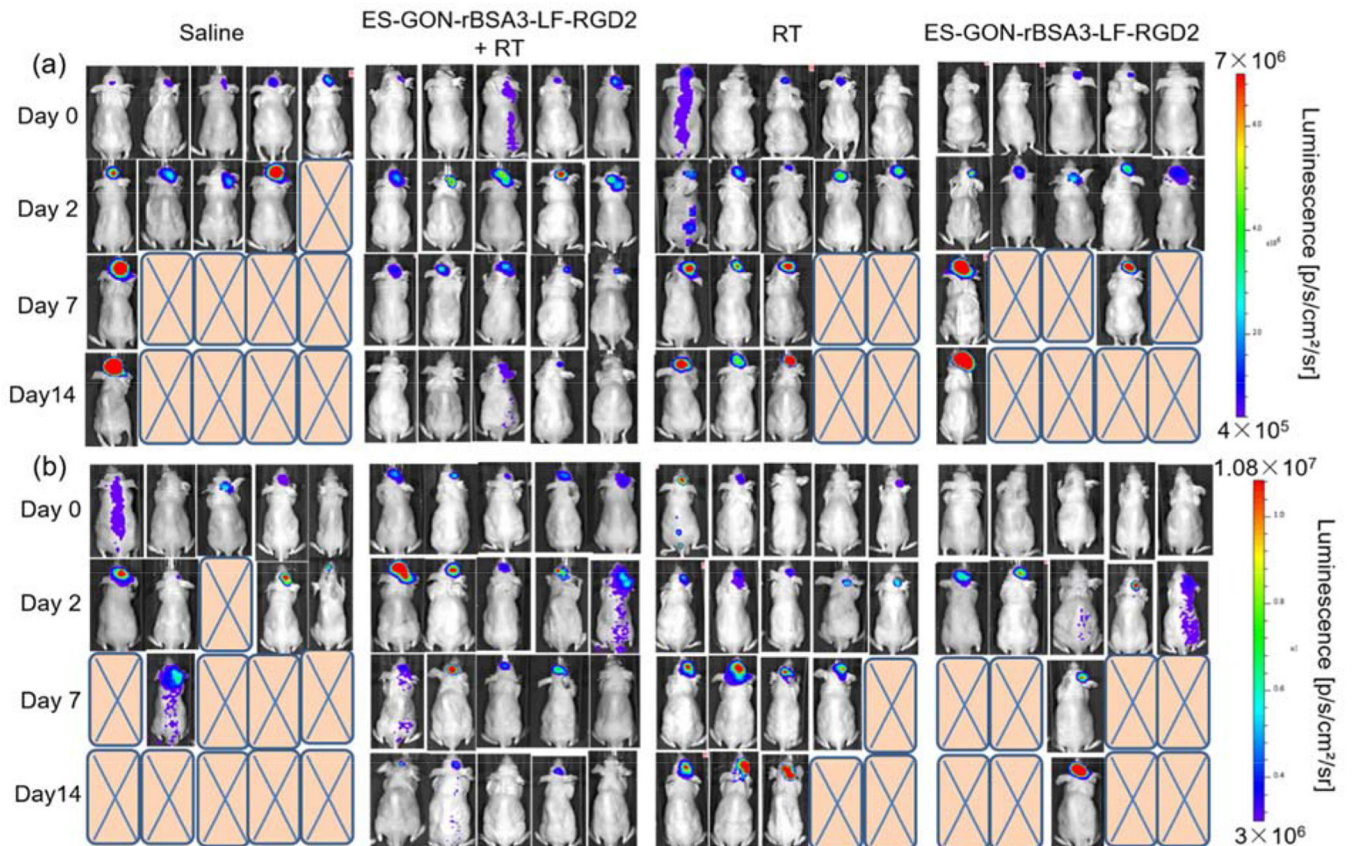
Figure 6.

(a, b): T_1-weighted MRI images of nude mice bearing subcutaneous U-87 MG tumors showing tumors (a) or livers (b) (slice orient: coronal). (c, d): Quantificational analysis of subcutaneous tumors (c) and livers (d) after intravenous injection of ES-GON-rBSA3-LF-RGD2. (e-g): Anti-tumor efficacies of ES-GON-rBSA3-LF-RGD2 on nude mice bearing subcutaneous U-87 MG tumors with or without irradiation of X-ray (6.0 Gy, 212 kVp) (mean ± SD, $n = 5$). (e): Changes of tumor volume. The mice were respectively treated with PBS (group 1), PBS plus X-Ray irradiation (group 2), ES-GON-rBSA3-LF-RGD2 (group 3), or ES-GON-rBSA3-LF-RGD2 plus X-Ray irradiation (group 4). * $P < 0.05$, ** $P < 0.01$, *** $P < 0.001$. (f): Survival rates of mice. Group 4 *vs.* group 1: $P = 0.002$; group 4 *vs.* group 3: $P = 0.002$. (g): Changes of the relative mouse body weight. Gd dose = 5.0 mg/kg.

Figure 7.
T_1-weighted MRI images of nude mice bearing orthotopic brain tumors scanned pre or post *i.v.* injection of Magnevist (a), ES-GON-rBSA3-RGD2 (b), or ES-GON-rBSA3-LF-RGD2 (c). The MRI images before injection are identified as "Pre". The Gd dosage is 5.0 mg/kg body weight.

Figure 8.
Bioluminescence images of nude mice bearing orthotopic U87-Luc glioblastoma (a) or orthotopic U251-Luc glioblastoma (b) with different treatments. The Gd dosage is 5.0 mg/kg. The ES-GON-rBSA3-LF-RGD2 treatment with irradiation of X-ray induced obvious therapeutic efficiency to the tumor, but other treatments (control) did not result in therapeutic efficiency to the tumor.

Table 1.

r_1 and r_2 measured using different MRI scanner systems.

Sample Nomenclature	H_0 (T)[a]	r_1 (mM^{-1} s^{-1})	r_2 (mM^{-1} s^{-1})	r_2/r_1[b]
Magnevist®	7.0	3.6	5.4	1.5
	1.5	4.3	4.6	1.1
ES-GON-rBSA3	7.0	18.6	64.0	3.4
	1.5	64.5	76.6	1.2
ES-GON-rBSA3-LF-RGD2	7.0	15.1	59.0	3.9
	1.5	60.8	67.3	1.1

[a]The r_1 and r_2 were determined using a MRI scanner system (7.0 T, Bruker, B-C 70/16 US), or a clinical MRI scanner system (1.5 T, Magnetom Avanto, Siemens, Germany) (mean ± S.D., $n = 3$).